Spatial Variation of Energy Resolution in 3-D Position Sensitive CZT Gamma-Ray Spectrometers

W. Li[1,2], Z. He[2], G.F. Knoll[2], D.K. Wehe[2], C.M. Stahle[3]
[2]Department of Nuclear Engineering and Radiological Sciences,
University of Michigan, Ann Arbor, MI 48109, U.S.A.
[3]Orbital Sciences Corp./NASA Goddard Space Flight Center,
Code 553, Greenbelt, MD 20771, U.S.A.

Abstract

This paper reports the energy resolutions obtained from two 3-D CZT γ-ray spectrometers. Each device is a 1 cm^3 cube CZT crystal with an 11×11 pixellated anode. For single-interaction events in the detector, the gamma ray interaction location can be determined in 3-D. With the volume of each detector conceptually divided into 11×11×18 voxels, the spectra of single-interaction events from each of the voxels were collected. The energy resolutions at 662 keV from a single voxel are typically 9.3 keV and 9.9 keV for the two detectors, with electronic noise contributing ~7 keV and ~6 keV respectively. A spatially-varying energy resolution has been observed for both detectors, which accounts for the degradation of energy resolution of the overall spectrum combined from all the voxels. The causes for the variations have been analyzed, and the impact of a spatially-varying energy resolution on a CZT gamma-ray spectrometer has been investigated.

I. Introduction

The γ-ray energy resolution of CZT room temperature detectors has been greatly improved by applying the single-polarity charge sensing technology[1]. Single-polarity charge sensing mitigates the problem of hole trapping, but the problems of electron trapping and material nonuniformity limit the energy resolution especially for detectors with the sufficiently large volume needed for γ-ray applications. While depth sensing provides a single correction for any electron trapping and nonuniformity in the depth direction[2], any material nonuniformity in the lateral direction can not be corrected. However, a unique 3-D position-sensing approach makes a full 3-D correction possible[3]. This approach was applied to comparatively large volume detectors and yielded energy resolution normally only available from small volume detectors.

Two CZT detectors have been developed for 3-D position sensing[3], each being a 1 cm^3 discrimination-grade CZT crystal with an 11×11 pixellated anode. The signals from the anode pixels are read out by an integrated VA1 readout chip with 128 independent signal processing channels. The cathode signal is read out by a separate preamplifier. For incident γ rays which interact at only one location, the interaction location in the lateral dimension (i.e., parallel to the plane of the electrodes) is determined by the position of the anode pixel producing the signal, and the depth is given by the ratio of the signals from the cathode and the anode pixel. Based on this 3-D position sensing method, the volume of the detector is conceptually divided into 11×11×18 voxels, and the γ-ray spectra of single-interaction events from each voxel are collected simultaneously. A volumetric distribution of the photopeak centroid location is obtained from the voxel-based spectra. After the normalization of photopeak centroid to account for volumetric nonuniformity, the spectra from all voxels are combined to yield a spectrum from the whole bulk of the detector. The energy resolution in the combined spectrum depends on the energy resolution and centroid normalization adjustment for each voxel-based spectrum.

In our experiments, software is used to perform the spectrum gain adjustment effectively. The ^{137}Cs spectra of single-pixel events (which account for ~25% of the photopeak events and ~45% of the total interaction events in the detector) were used to obtain the spatial variation of the energy resolution in the two 3-D CZT detectors. Since the energy resolutions from the voxels under the same anode pixel may not be independent (i.e., the energy resolution from a voxel may be influenced by the electron trapping in the voxels between it and the anode pixel), the spectra from each pixel were first combined and the pixel-based variation of energy resolution was investigated along the lateral dimension. Degradation of energy resolution has been observed in peripheral pixels and some central pixels for both detectors. Voxel-based energy resolutions were measured under different cathode biases to investigate the possible causes for the spatially-varying energy resolution.

II. 3-D Nonuniformity Correction

To correct for nonuniformity in the detector bulk, we divided the detector into $i \times j \times k$ voxels, where $i \times j$ is the number of anode pixels and k is the number of depth layers we choose to consider. Even if the response from the detector were uniform, the measured signal amplitude will have variations due to the difference in the gains of each individual electronic channel. Denote this electronic gain variation, which can be measured separately, as f^e_{ij}. The 3-D variation in the electron generation (e.g., due to nonuniform zinc concentration[4]) and collection is given by f^d_{ijk}. With energy deposition E_{ijk} in voxel (i,j,k), the signal measured on pixel (i,j) should be:

$$V_{ij}(k) = f^e_{ij} \cdot f^d_{ijk} \cdot E_{ijk} = f_{ijk} \cdot E_{ijk} \qquad (1)$$

where the overall variation of f_{ijk} is independent of the energy deposition. For monoenergetic γ rays of energy E, f_{ijk}

[1]E-mail: wenli@engin.umich.edu

0018-9499/99$10.00

can be determined from the measured photopeak centroids for all voxels as: $V_{ij}^{centroid}(k)/E$.

A. Calibration

The purpose of calibration is to measure the 3-D variation of the photopeak centroid and determine f_{ijk} used in the nonuniformity correction. An accurate calibration usually takes a few days in our current system because of the small volume of each voxel and the long dead time of the readout system. Since variations in f_{ijk}^{d} are influenced by different amounts of electron trapping along the depth, a calibration has to be performed for each cathode bias. While a temperature-dependence of f_{jk}^{e} has been observed[5], the temperature effect across all VA1 channels is quite uniform and will not influence the relative variation of f_{ijk}. Thus, a single calibration was used under varying ambient temperatures without loss of resolution.

B. Spectrum Gain Adjustment for Discrete Channels

The gain adjustment $1/f_{ijk}$ needs to be applied to the spectrum from each voxel before these spectra can be combined. It is difficult to do the gain adjustment before the A/D conversion. We also can not simply apply the adjustment coefficient to the A/D conversion result because of distortions caused by round-off error. In our experiments the gain adjustment is performed in the following manner. Assuming the original spectrum is collected with an ADC channel width of ΔV and the nonlinearities in the A/D conversion are negligible, the boundaries of the ith channel should be $V_{i-1} = (i-1)\cdot\Delta V$ and $V_i = i\cdot\Delta V$. Applying a gain correction coefficient G to the original spectrum is equivalent to changing the channel width to $\Delta V' = \Delta V/G$. The new spectrum has channel boundaries $V_j' = j\cdot\Delta V'$, and the count number in the new jth channel is calculated assuming the count density $(N_i/\Delta V)$ is constant in each original channel (cf. Fig. 1). If N_i and N_j' are the counts in channel i of the original spectrum and channel j in the new spectrum respectively, and the boundaries of the jth channel in the new spectrum satisfy $V_{i-2} < V_{j-1}' < V_{i-1} < V_j' < V_i$, then the count number N_j' can be calculated as:

$$\begin{aligned} N_j' &= N_{i-1}\frac{V_{i-1}-V_{j-1}'}{\Delta V} + N_i\frac{V_j'-V_{i-1}}{\Delta V} \\ &= N_{i-1}(i-1-\frac{j-1}{G}) + N_i(\frac{j}{G}-(i-1)) \quad (2) \end{aligned}$$

The mapped spectrum is only determined by the related channel numbers and the coefficient G. Fig. 2 shows the result of a gain adjustment to a measured ^{137}Cs spectrum. The gain adjustment is applied to the original spectrum (A) to move the photopeak centroid to channel 1000 and yield spectrum (B). The effect of an identical gain adjustment on a rectangular distribution is also shown in Fig. 2. No obvious distortion is observed with this gain adjustment method and the total counts are preserved.

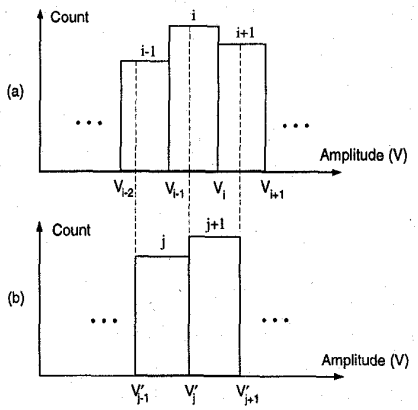

Figure 1: Calculation of the new count number of a channel in the gain adjustment. (a) the original spectrum (b) the new spectrum

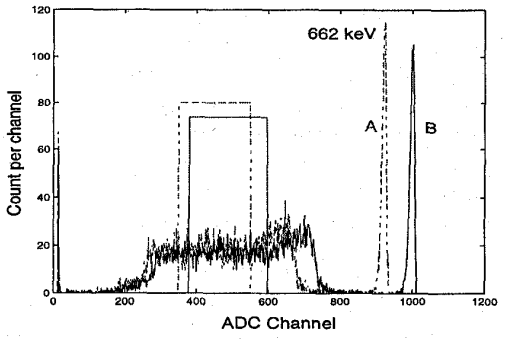

Figure 2: Result of gain adjustment for a ^{137}Cs spectrum.

III. Experimental Results and Discussions

To collect voxel-based ^{137}Cs spectra of single-pixel events from the two 3-D CZT detectors, a 10 μCi ^{137}Cs source irradiated the detector from the cathode side. The highest cathode bias in the two detectors is limited by leakage current saturating the VA1 chip, and was -2400 V (detector #1) and -1400 V (detector #2). Because the electronic noise of the readout system is ~7 keV (FWHM), the energy threshold used to distinguish the single-pixel events was set to ~8 keV. In depth sensing, the number of depth layers is set to 18 in the spectra collection since the measured depth resolution is about 5

A. Calibration and the Spectrum from a Pixel

While the relative variations in f_{ijk} should be temperature independent, the overall detector response (and each value of f_{ijk}) will change with temperature and degrade the energy resolution. To compensate for this effect during the long calibration runs, a peak-based spectrum stabilization technique[5] was implemented using the spectrum derived from the entire detector volume. This approach maintains $V_{ij}^{centroid}(k)$ approximately constant during the runs.

Fig. 3 shows the calibration spectra from a normal pixel (pixel #6) of detector #1. The calibration was performed for ~60 hours with a cathode bias of -2000 V. Except for

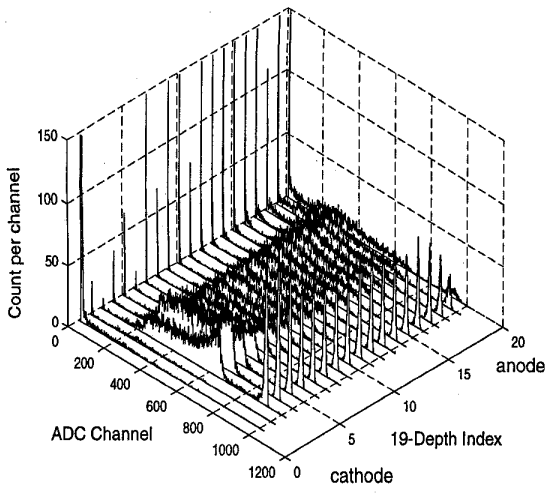

Figure 3: ^{137}Cs spectra of single-pixel events from the pixel #6 of 3-D CZT detector #1.

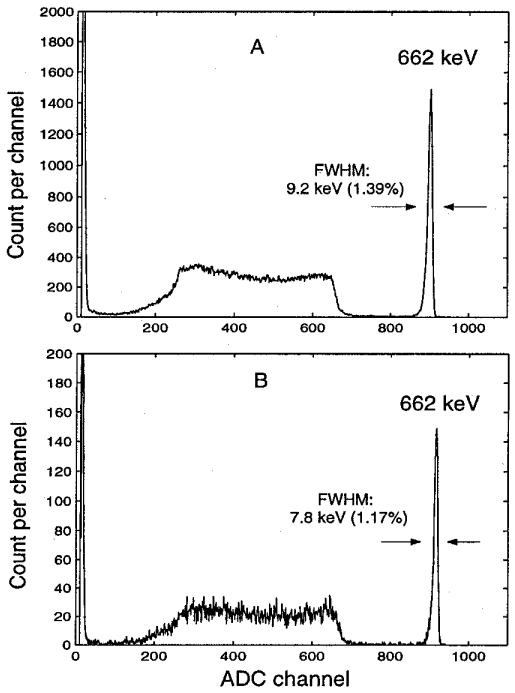

Figure 4: ^{137}Cs combined spectrum of single-pixel events from pixel #6 of CZT detector #1 after nonuniformity correction along the depth. A: self-calibrated(~60 hours) B: ~6 hours

the spectra from the nonlinear region near the anode, the photopeak area exceeds 1000 counts for each spectrum and the uncertainty in photopeak centroid determination is smaller than 0.1%(FWHM). Using the f_{ijk} derived from this calibration, all the spectra from this pixel were combined to yield Spectrum A in Fig. 4. Another set of spectra was collected over ~6 hours from detector #1 without as much variation in ambient temperature. The combined spectrum from pixel #6 using the same f_{ijk} values is shown as Spectrum B in Fig. 4. Comparing the energy resolutions from the two combined spectra, we can see that the degradation of energy resolution caused by the temperature effect is noticeable even with spectrum stabilization applied.

B. Variation of FWHM in Lateral Dimension

Using a set of spectra collected over ~6 hours from detector #1, the spectra from each pixel were combined using the calibration factors f_{ijk} measured over ~60 hours. The histogram and lateral distribution of the FWHM from each pixel are shown in Fig. 5 for detector #1 and fig. 6 for detector #2. Significant degradations of energy resolution are observed in most peripheral pixels and some central pixels. The electronic noise of each VA1 channel was measured, and the energy resolution after the subtraction of electronic noise was calculated for each pixel. The relative variation of the results is quite similar to that in Fig. 5, which implies that the cause of the variation is from the detector.

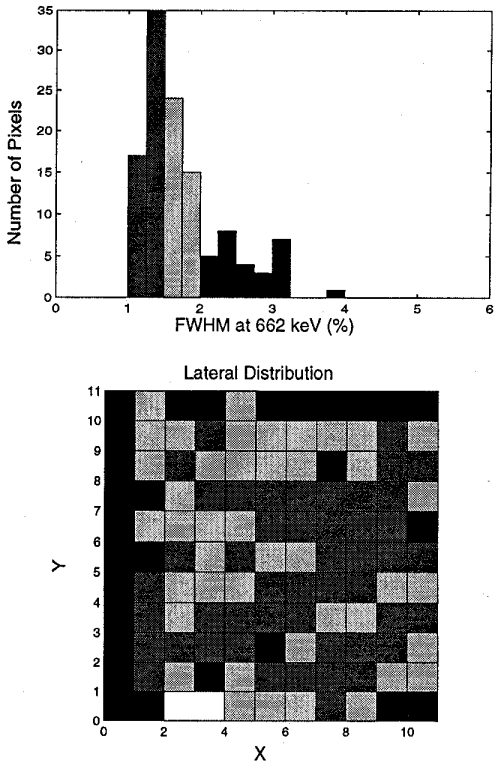

Figure 5: Lateral pixel-based distribution of FWHM at 662 keV for single-pixel events from the 3-D CZT detector #1.

For the peripheral pixels, the degradation of energy resolution can be explained by the gap between the anode pixel and the edge of CZT crystal. Electrons generated in this gap still can be collected at the nearest peripheral pixel (in fact, the photopeak count rates of peripheral pixels are higher than that of central pixels), but have a longer trajectory and drifting time and hence poorer collection efficiency. In detector #1, the gap corresponding to the peripheral pixels with $x = 1$ or $y = 11$

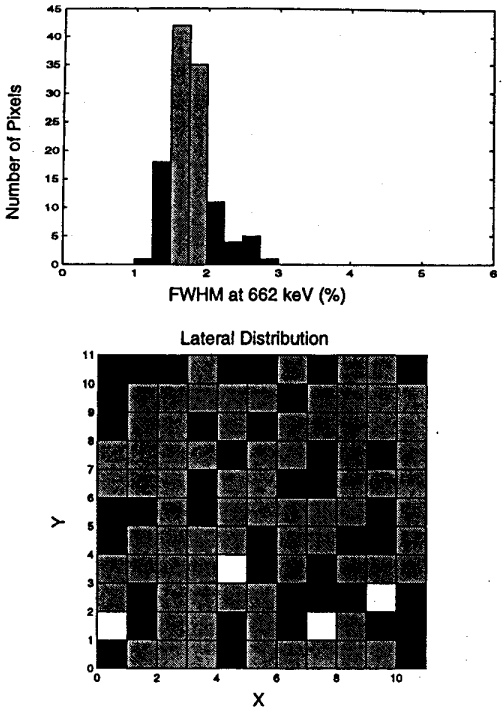

Figure 6: Lateral pixel-based distribution of FWHM at 662 keV for single-pixel events from the 3-D CZT detector #2.

is about 1.5 times as wide as that corresponding to the pixels with $x = 11$ or $y = 1$ (see Fig. 5). This explains why energy resolution degradation is less serious along those edges.

C. *Voxel-based Energy Resolution*

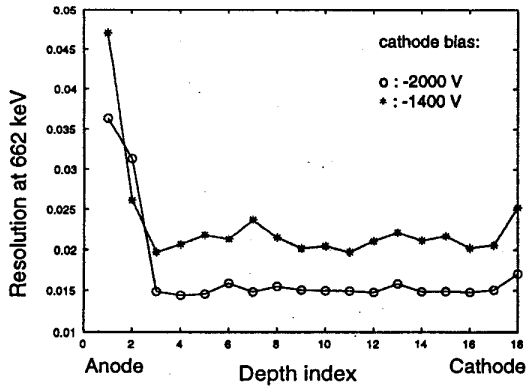

Figure 7: Voxel-based distribution of FWHM at 662 keV from pixel #6 (x=4,y=3) of detector #1.

The voxel-based distribution of energy resolution along the depth for pixel #6 of detector #1 is shown in Fig. 7 for two applied biases. With increased cathode bias the FWHM is improved uniformly along the depth (except for the nonlinear region near the anode). Reduced electron trapping nonuniformity in lateral dimension can explain the improved FWHM near the cathode side, but not for the improvement near the anode (cf. depths ~3-6 on fig. 7). The cause of this effect is currently being investigated.

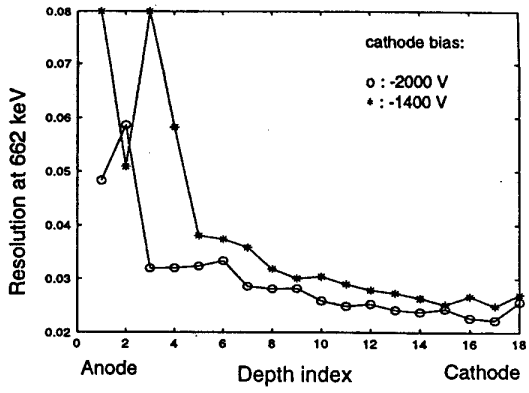

Figure 8: Voxel-based distribution of FWHM at 662 keV from pixel #101 (x=1,y=8) of detector #1.

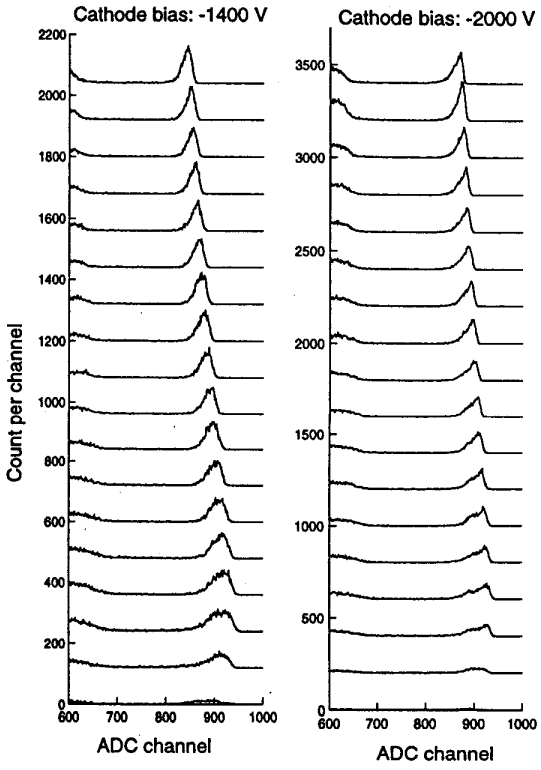

Figure 9: Photopeaks in voxel-based ^{137}Cs spectra of single-pixel events from pixel #101 (x=1,y=8) of detector #1. From the upper to the lower: from the cathode to the anode.

Fig. 8 shows the voxel-based distribution of energy resolution from a typical peripheral pixel (x=1, y=8) of detector #1, and the corresponding spectra are shown in Fig. 9. The energy resolution in the peripheral pixels is degraded by events from the gap between the pixel and the edge of CZT crystal. The decreasing FWHM for events further from the anode implies decreasing difficulty for electrons in the gap to move in the lateral dimension and be collected. This is probably due to having a detector with a smaller anode (7.7×7.7 mm^2) than

cathode (10×10 mm^2). From Fig. 9 we can also see the improved FWHM with increased cathode bias is primarily from the sharper high energy tails of the photopeaks. This suggests that the improved FWHM is from the volume directly under the pixel, and shows the potential FWHM which could be acquired from the peripheral pixels if we could eliminate the contributions from events originating in the edge gaps in the current detector.

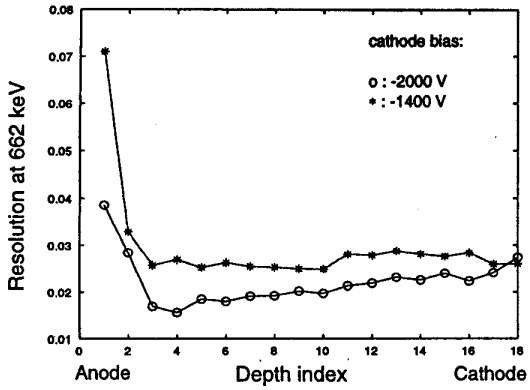

Figure 10: Voxel-based distribution of FWHM at 662 keV from pixel #106 (x=4,y=6) of detector #1.

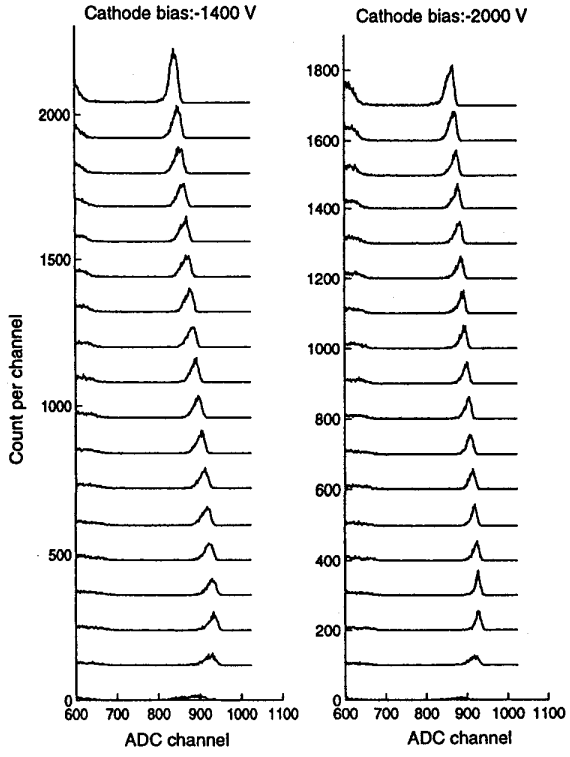

Figure 11: Photopeaks in voxel-based ^{137}Cs spectra of single-pixel events from pixel #106 (x=4,y=6) of detector #1. From the upper to the lower: from the cathode to the anode.

In contrast to the normal central and peripheral pixels, those central pixels having poor energy resolution have a monotonously increasing FWHM along the depth from the anode to the cathode. Fig. 10 shows the distribution of FWHM from one of these pixels in detector #1, and the corresponding spectra are shown in Fig. 11. The monotonously increasing FWHM from the anode to the cathode implies the existence of a defective region having unusual electron trapping nonuniformity. This will contaminate all the spectra from the volume between this region and the cathode. This situation can only be improved by choosing a better quality crystal from which to fabricate the detector.

D. Energy Resolution from the Global Spectra

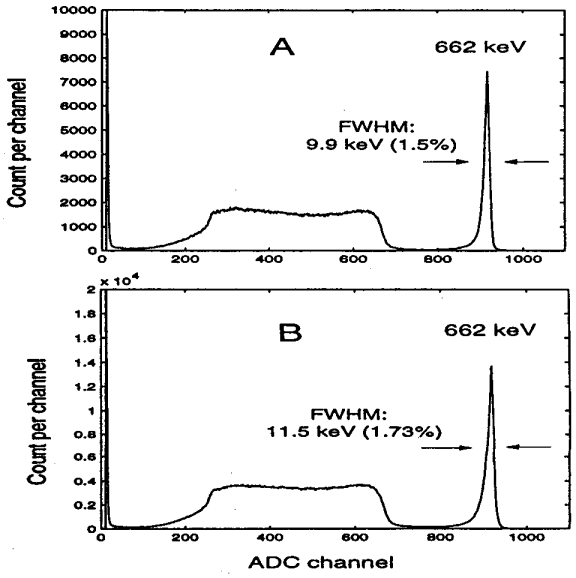

Figure 12: ^{137}Cs combined spectrum of single-pixel events from 3-D CZT detector #1 after 3-D correction. A: from the 9×9 central pixels. B: from the whole bulk.

Fig. 12 and 13 show the ^{137}Cs combined spectra from the 9×9 central pixels and the whole bulk of the detector #1 and #2. Compared with the FWHM of 7.8 keV (1.17%) from a normal pixel shown in Fig. 4 for detector #1, the FWHM increases to 9.9 keV (1.5%) for the combined spectrum from the 9×9 central pixels, and further increases to 11.5 keV (1.73%) for the combined spectrum from the whole bulk of the detector. The spatial variation of the energy resolution detailed above accounts for the degradation of energy resolution from the combined spectra. But the unique 3-D position sensitivity provides the flexibility of identifying those voxels with poor energy resolution in the calibration measurement, and then excluding their contributions from the overall spectrum in future measurements. As an example, excluding the contribution from the peripheral pixels brings obvious improvement to the energy resolution of the combined spectrum.

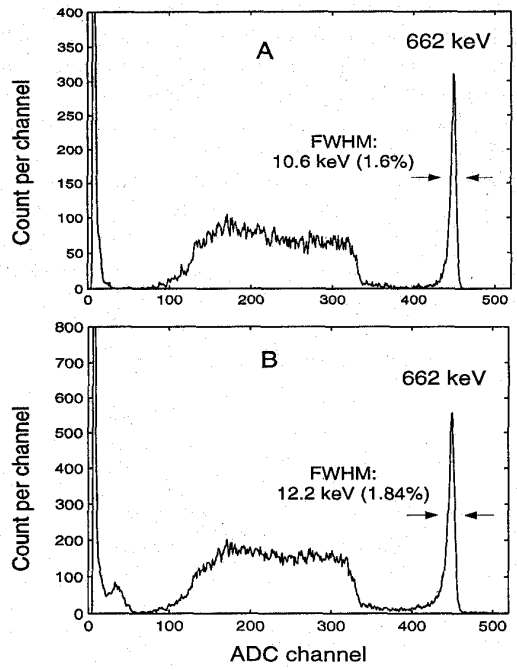

Figure 13: ^{137}Cs combined spectrum of single-pixel events from 3-D CZT detector #2 after 3-D correction. A: from the 9×9 central pixels. B: from the whole bulk.

IV. Summary and Conclusion

In the experiment with two 3-D position sensitive CZT spectrometers, voxel-based ^{137}Cs spectra of single-pixel events were collected and combined. The spectra combined from the whole bulk of the detectors yield the FWHM of 11.5 keV (1.73%) and 12.2 keV (1.83%) at 662 keV for the two detectors. Significant degradation of energy resolution was observed from the peripheral pixels and some central pixels in both of the detectors. The degradation of energy resolution in peripheral pixels is due to the gaps between the anode electrode and the boundary of the CZT crystal. The degradation of energy resolution in central pixels is believed to be dominated by the nonuniformity of electron trapping along the collection path. For future detectors, the anode pattern will be revised to minimize the gaps between the peripheral pixels and the edge of the CZT crystal, and CZT crystals with better material uniformity should be used instead of the current discrimination grade crystals. With these two improvements, one can expect a more uniform distribution of energy resolution along both lateral and depth dimensions, and hence, better energy resolution from the whole bulk of the detector.

V. Acknowledgments

This work was supported under DOE Grant DOE-FG08-94NV13357.

VI. References

[1] P.N. Luke, "Unipolar Charge Sensing with Coplanar Electrodes–Application to Semiconductor Detectors", IEEE Trans. Nucl. Sci., Vol. 42, No. 4, pp. 207-213, Aug. 1995

[2] Z. He, et al., "1-D Position Sensitive Single Carrier Semiconductor Detectors", Nuclear Instruments and Methods, Vol. A380, pp. 228-231, 1996.

[3] Z. He, et al., "3-D Position Sensitive CdZnTe Gamma-Ray Spectrometers", *1998 Symposium on Radiation Measurements and Applications,* Ann Arbor, Michigan, 1998.

[4] J.E. Toney, et al., "Uniformity of $Cd_{1-x}Zn_xTe$ Grown by High-pressure Bridgman", Nuclear Instruments and Methods, Vol. A380, pp. 132-135, 1996.

[5] W. Li, et al., "A data Acquisition and Processing System for 3-D Position Sensitive CZT Gamma-Ray Spectrometers",, *IEEE Nuclear Science Symposium,* Toronto, Canada, 1998.